Available online at www.sciencedirect.com

ScienceDirect

Current Opinion in Electrochemistry

Review Article

Electrocatalysis at the polarised interface between two immiscible electrolyte solutions

Alonso Gamero-Quijano[1], Grégoire Herzog[2], Pekka Peljo[3] and Micheál D. Scanlon[4]

Abstract

Electrocatalysis at the interface between two immiscible electrolyte solutions (ITIES) is an emerging field of research, which allows the separation of reactants according to their lipophilicity. Electrocatalysts of various natures (noble metals, carbon-based and inorganic nanomaterials, enzymes, and supramolecular ensembles) are assembled at the ITIES, either spontaneously or following the application of an interfacial Galvani potential difference. While primarily used for the electrocatalysis of the oxygen reduction reaction (ORR) and hydrogen evolution reaction (HER), recent work has focused on the electrocatalysis of the oxygen evolution reaction (OER) and the electrocatalytic oxidation of elemental sulfur (S_8) and an organosulfur compound. Protocols to compare electrocatalytic performances at the ITIES call for careful data analysis and a detailed knowledge of the catalyst's morphological parameters (*e.g.,* active surface area and catalyst loading). However, standardisation of such protocols at the ITIES has yet to be implemented and is required to allow better comparison of the results from individual biphasic systems.

Addresses

[1] Department of Physical Chemistry, University of Alicante (UA), E-03080, Alicante, Spain

[2] Université de Lorraine, CNRS, LCPME, F-54000 Nancy, France

[3] Research Group of Battery Materials and Technologies, Department of Mechanical and Materials Engineering, Faculty of Technology, University of Turku, 20014 Turun Yliopisto, Finland

[4] The Bernal Institute and Department of Chemical Sciences, School of Natural Sciences, University of Limerick (UL), Limerick V94 T9PX, Ireland

Corresponding authors: Gamero-Quijano, Alonso (daniel.gamero@ua.es); Herzog, Grégoire (gregoire.herzog@cnrs.fr); Peljo, Pekka (pekka.peljo@utu.fi); Scanlon, Micheál D. (micheal.scanlon@ul.ie)

Current Opinion in Electrochemistry 2023, **38**:101212

This review comes from a themed issue on **Electrocatalysis**

Edited by **Galina A. Tsirlina** and **Elena R. Savinova**

For a complete overview see the Issue and the Editorial

Available online 19 January 2023

https://doi.org/10.1016/j.coelec.2023.101212

Keywords

Electrocatalysis, Polarised liquid|liquid interfaces, Interface between two immiscible electrolyte solutions, Hydrogen evolution reaction, Oxygen reduction reaction, Oxygen evolution reaction.

Introduction

Biphasic systems allow the electrocatalysis of reactants which are separated according to their lipophilicity [1]. Catalytic nanomaterials and supramolecular films can be assembled at the polarised Interface between Two Immiscible Electrolyte Solutions (ITIES) spontaneously, or by the application of an external driving force, *e.g.*, in the form of an interfacial Galvani potential difference ($\Delta_o^w\phi$) [2–7]. Furthermore, electrochemistry at the ITIES allows direct probing of the electrocatalytic activity of the nanomaterials or films free from the influence of an underlying support [8].

The two main electrocatalytic processes investigated at the ITIES to date, using metallic or inorganic nanomaterials, are of the energy-related oxygen reduction reaction (ORR) [9–15] and hydrogen evolution reaction (HER) [16–34]. The electrocatalytic oxidation of elemental sulfur (S_8) and the organosulfur compound 2,5-dimercapto-1,3,4-thiadiazole (DMcT) by gold nanoparticles (AuNPs) [35,36], photoelectrocatalysis of the oxygen evolution reaction (OER) [37–43], HER [44–49], and ORR [50–57] by a series of diverse strategies, and bioelectrocatalysis of the ORR using the redox-active protein cytochrome *c* (Cyt *c*) [58,59] at the ITIES have also been reported. In this review, recent progress for each of these biphasic electrocatalytic processes is overviewed. An in-depth discussion is also provided on the need for stricter standard protocols for electrocatalysis at the ITIES, to allow better comparison of the results from individual biphasic systems. Electrocatalysis of the ORR at the ITIES using molecular catalysts, such as cobalt or iron porphyrins and phthalocyanines dissolved in the aqueous phase, is not discussed in detail herein, as a detailed description of this research is provided in a recent review by Opallo et al. [60].

Electrocatalysis at the ITIES by metallic, carbon-based, or inorganic nanomaterials

In the liquid|liquid interface configuration, both the ORR and HER require: (i) a lipophilic electron donor dissolved in the organic phase, which is typically a ferrocene derivative (ferrocene Fc, dimethylferrocene DiMFc, or decamethylferrocene DcMFc) or tetrathiafulvalene; and (ii) protons available from the aqueous phase and oxygen dissolved in either phase to diffuse freely towards the 2D or 3D assemblies of catalysts. Although the interfacial electron transfer (IET) reaction is thermodynamically possible between the oxidising species dissolved in the aqueous phase (H^+ or O_2) and the electron donor present in the organic phase, the reaction kinetics are greatly improved by the presence of nanocatalysts in the ITIES. Thanks to Fermi level equilibration, conducting nanoparticles (NPs) adsorbed at the ITIES allow direct electron transfer by acting as bipolar electrodes and facilitating catalytic reactions [12,61]. Catalytically improved electron transfer through an AuNP film was demonstrated through the investigation of electron transfer between lipophilic ferrocenium cation/ferrocene and hydrophilic ferri-ferrocyanide redox couples (Figure 1a(i)) [62]. The peak-to-peak separation was greater than 90 mV in the absence of a catalyst (Figure 1a(ii)) but decreased down to 70 mV when the AuNP film was present at the ITIES (Figure 1a(iii)).

Catalysts made of noble metals (*e.g.*, Au [10,12], Pt [14], and Pd [10]) or purely carbon-based (*in situ* generated reduced graphene oxide [11], graphene [13] and even lithium-ion battery waste [15]) were mainly used for the ORR, whereas a larger selection of inorganic materials were tested for the HER: MoS_2 [16,17,27,28,31,32] Mo_2C [18,19], Cu [21,25,34], Cu_2CoSnS_4 [22], Cu_2WS_4 [23], CoS [24], black phosphorus [33], NiS [26], W_2S [20] and W-based ternary metal sulfides [29]. These catalysts were adsorbed as such at the ITIES or were supported onto carbon-based materials, *e.g.*, carbon nanotubes [17,19,24–26] and reduced graphene oxide [27,34]. Carbon-based nanomaterials, on which the catalysts were immobilised, helped to efficiently transfer electrons between the lipophilic electron donor and the hybrid materials (and not exclusively from the catalytically active site) leading to an increased HER rate (Figure 1b).

Over the past decade, the study of single NPs by their collision with microelectrodes has been exploited to size NPs, determine their shape, and provide insights into NP agglomeration or aggregation phenomena [63,64]. Such single-entity electrochemical measurements at a micron-sized ITIES were demonstrated by Stockmann et al. [14] by recording current spikes, that were rationalised by a COMSOL 2D simulation, and attributed to the electrocatalytic ORR upon impact of Pt NPs at the ITIES with ferrocene acting as the electron donor (Figure 1c). A major advantage of this approach to single-entity electrochemistry is the more facile and reproducible preparation of microITIES, supported at the tip of a micropipette filled with either the aqueous or organic phase, *versus* microelectrodes [14,65]. Nevertheless, single-entity electrochemistry remains underexplored at microITIES *versus* microelectrodes due to the relatively small community of researchers actively working on this topic presently.

Suárez-Herrera et al. used a film of AuNPs at the ITIES to act as a catalytic surface onto which O_2 and elemental sulfur (S_8) can adsorb [35]. Electrocatalytic oxidation of S_8 by O_2 was then achieved by providing an electrochemical driving force through polarisation of the ITIES and tuning the Fermi level of the interfacial AuNPs by the adsorption of aqueous anions (Figure 1d). This system mimics biochemical sulfur oxidation under ambient conditions with the ITIES being the ideal environment to oxidise S_8, overcoming the incompatible solubilities of the hydrophobic reactants (O_2 and S_8) and hydrophilic products (H^+, SO_3^{2-}, SO_4^{2-}, *etc.*). In a separate study, Suárez-Herrera et al. also used a film of AuNPs at the ITIES to electrocatalyse the oxidation of the organic soluble organosulfur molecule 2,5-dimercapto-1,3,4-thiadiazole (DMcT) by O_2, yielding a floating interfacial AuNP/poly(DMcT) film by oxidative electrosynthesis [36]. Raman spectroscopy strongly suggested the AuNP/poly(DMcT) film is surface-enhanced Raman spectroscopy (SERS)-active and a coordination polymer of poly(DMcT) with AuNPs.

Photoelectrocatalysis at the ITIES

To date, all photoelectrocatalytic OER experiments at the ITIES have been performed with butyronitrile as the organic solvent due to its stability under strongly oxidising conditions [37–43]. Using a film of $BiVO_4$ photocatalyst with a specific hyperbranched structure at the ITIES, Rastgar et al. added $[Co(bpy)_3](PF_6)_3$ to the organic phase with the dual role of acting as the redox-active oxidant, scavenging conduction band electrons from $BiVO_4$ upon illumination and thereby enhancing the separation efficiency of photogenerated charge carriers, and as a scanning electrochemical microscopy (SECM) redox probe [37,38]. The latter permits the kinetics of the photoinduced interfacial electron transfer (IET) reaction to be probed by recording SECM feedback approach curves using a microelectrode that approaches the ITIES from the organic side and re-oxidises the photo-generated $[Co(bpy)_3]^{2+}$ (Figure 2a(i)). Additional SECM feedback approach curves directly detected the O_2 evolved upon oxidation of water by the valence band holes of $BiVO_4$ during illumination [38]. By tuning the applied $\Delta_o^w\phi$ by varying the concentration ratio of the potential determining perchlorate anion (ClO_4^-) in each phase, increased rates of $[Co(bpy)_3]^{2+}$

Figure 1

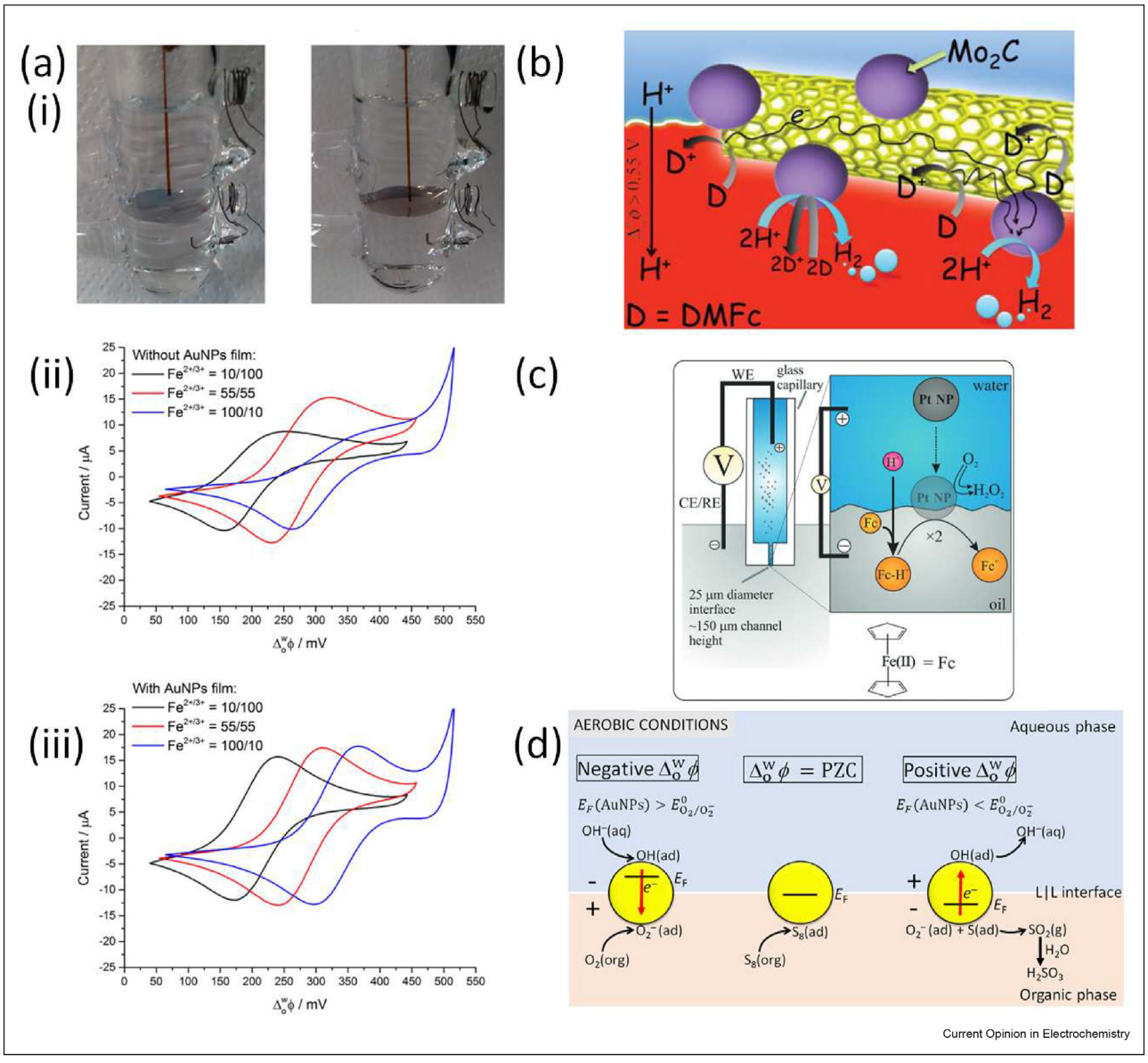

Electrocatalysis at the ITIES by metallic, carbon-based, or inorganic nanomaterials at the ITIES. (a) (i) Images of AuNP films prepared at a polarisable water|α,α,α-trifluorotoluene (TFT) interface in a four-electrode electrochemical cell using AuNPs with mean diameters of 12 nm (left panel) and 38 nm (right panel). **(ii), (iii)** Cyclic voltammograms of interfacial electron transfer between organic soluble ferrocenium cation/ferrocene and aqueous soluble ferri-ferrocyanide redox couples, with various ratios between Fe^{2+} and Fe^{3+} investigated, both **(ii)** in the absence and **(iii)** in the presence of an interfacial AuNP nanofilm. The scan rate used was 10 mV s^{-1}. **(b)** Schematic of the biphasic HER in the presence of a CNT/Mo_2C nanocomposite adsorbed at a polarisable liquid|liquid interface. The electron donor, decamethylferrocene (DcMFc), may inject electrons anywhere on the carbon support and not necessarily directly at the Mo_2C active site. **(c)** Schematic of a Pt NP impact leading to a measurable current spike at a micron-sized ITIES due to the electrocatalysis of the biphasic ORR using ferrocene as the electron donor. **(d)** An overview of the electrochemically driven biphasic sulfur oxidation reaction under aerobic conditions when the interfacial Galvani potential difference ($\Delta_o^w\phi$) is polarised negatively, positively, or equal to the potential of zero charge (PZC). **(a)** is reproduced with permission from ref. [62]. Copyright 2015 American Chemical Society. **(b)** is reproduced from ref. [19] with permission from the Royal Society of Chemistry. Copyright 2013. **(c)** is reproduced with permission from ref. [14]. Copyright 2017 Wiley-VCH. **(d)** is reproduced from ref. [35] with permission from Elsevier. Copyright 2022.

Figure 2

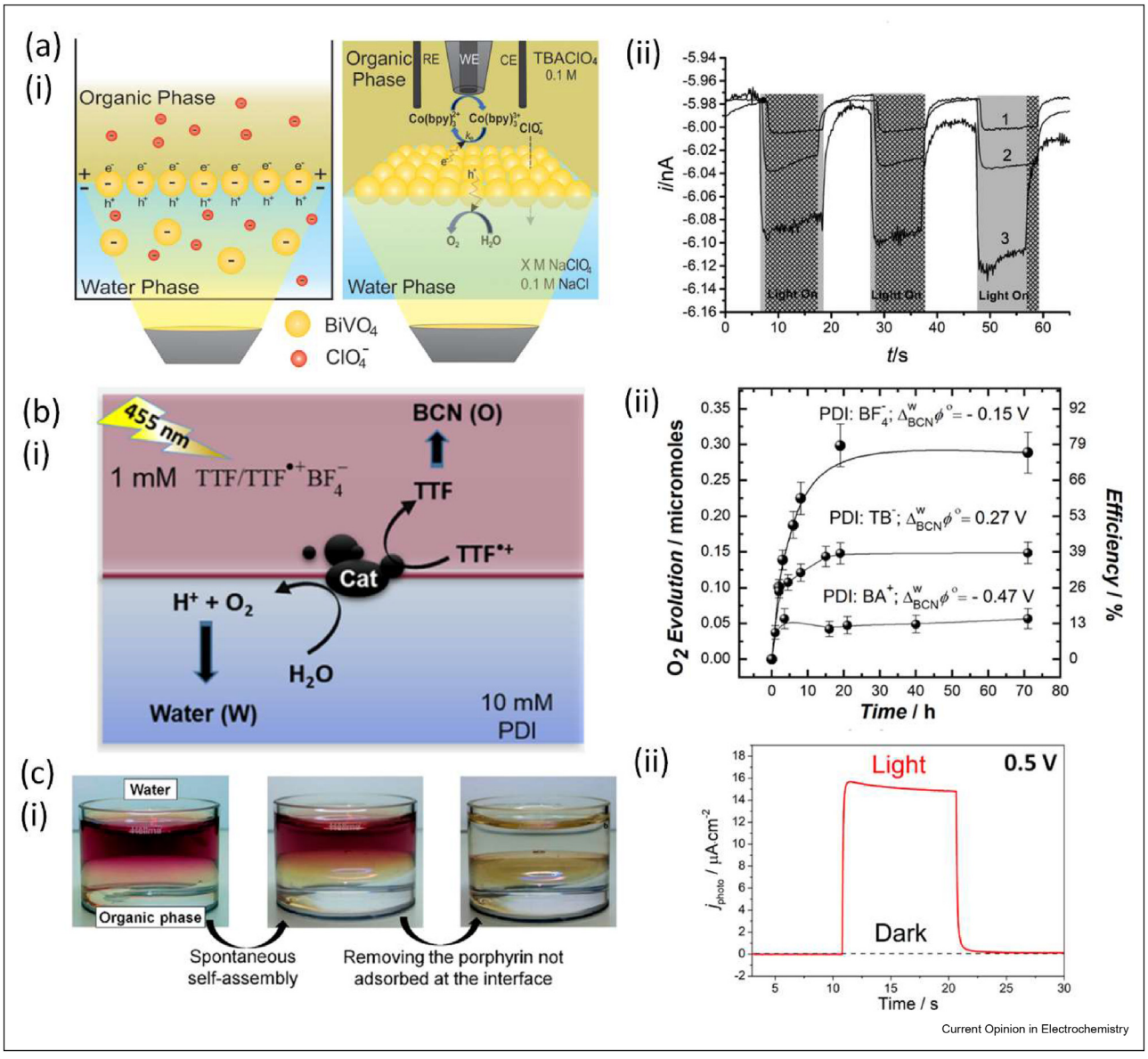

Photoelectrocatalysis at the ITIES. (a) (i) Schematic of scanning electrochemical microscopy (SECM) approach curves for the photoelectrocatalytic O_2 evolution reaction (OER) using a film of $BiVO_4$ photocatalyst at the ITIES and organic soluble $[Co(bpy)_3]^{2+}$ as both a sacrificial oxidant and SECM redox probe. **(ii)** Photocurrent transients of increased magnitude upon reduction of O_2 at a microelectrode positioned in the organic phase at a fixed distance away from the ITIES as the applied $\Delta_o^w\phi$ was tuned to less positive potentials using perchlorate anions (ClO_4^-) as the potential determining ion (PDI); the $[ClO_4^-]_{aq.}/[ClO_4^-]_{org.}$ ratios are 1:1, 1:2 and 1:10 for the transients labelled 1, 2 and 3, respectively. **(b) (i)** Composition of a biphasic cell used to evaluate the effect of polarisation of an aqueous|butyronitrile (BCN) interface on the photoelectrocatalytic OER by tetrathiafulvalene (TTF), $TTF^{\bullet+}$ and tetrafluoroborate anions (BF_4^-) molecular assemblies adsorbed on the surface of Pt microparticles. **(ii)** O_2 produced in the biphasic cells described in **(b) (i)** with BF_4^-, tetrakis(pentafluorophenyl)borate anions (TB^-) or bis(triphenylphosphoranylidene)ammonium cations (BA^+) as the PDI. The O_2 evolved was quantified by sampling the headspace of septum-sealed glass vials using a lock-in syringe with a push−pull valve and injecting the sample on to a gas chromatography-mass spectroscopy (GC-MS) instrument. **(c) (i)** Optical images of the formation of a film of ZnTPPc interfacial nanostructures at an aqueous|α,α,α-trifluorotoluene (TFT) interface with the pH of the aqueous phase precisely matching the p*K*a of the carboxyphenyl-substituents (pH 5.8). **(ii)** Comparison of photocurrent transients due to the phootoelectrocatalytic O_2 reduction reaction (ORR) measured in the presence of a film of ZnTPPc interfacial nanostructures with and without LED illumination, at an applied $\Delta_o^w\phi$ of 0.5 V with decamethylferrocene as the organic electron donor. The supporting organic electrolyte was bis(triphenylphosphoranylidene)ammonium tetrakis(pentafluorophenyl)borate (BATB). **(a)** is reproduced with permission from ref. [38]. Copyright 2017 American Chemical Society. **(b)** is reproduced from ref. [42] with permission from Elsevier. Copyright 2022. **(c)** is reproduced with permission from ref. [57]. Copyright 2020 American Chemical Society.

oxidation and O_2 reduction were recorded as the applied $\Delta_o^w\phi$ shifted to less positive potentials. These observations may be due to an increased thermodynamic driving force for the photoelectrocatalytic OER (*i.e.*, following Butler-Volmer theory), more efficient electron-hole separation, or an increased surface coverage of $BiVO_4$. The photoelectrocatalytic effect of the $BiVO_4$ nanoparticles was further demonstrated by obtaining photocurrent transients upon reduction of O_2 at a microelectrode positioned in the organic phase at a fixed distance away from the ITIES (Figure 2a(ii)) [38]. Additionally, the formation and decay of the $OH^\bullet$ intermediates during the OER at the surface of the $BiVO_4$ nanoparticles was quantified *in situ* by a surface interrogation mode of SECM involving the approach of a microelectrode to a micropore orifice that supported the $BiVO_4$ modified ITIES [39].

Girault and co-workers employed *in situ* self-assembled *p*-type semiconductors, consisting of tetrathiafulvalene (TTF), $TTF^{\bullet+}$ and BF_4^- or PF_6^- molecular assemblies adsorbed on the surface of Co_3O_4 or Pt nanoparticles, as an electron acceptor/photosensitiser redox OER photoelectrocatalyst at the ITIES (Figure 2b(i)) [40–42]. Initial studies in a non-polarisable fully miscible water/acetonitrile system were hampered by protonation of the molecular assemblies, triggering competing reactions such as the HER and ORR, and preventing electrochemical recycling of $TTF^{\bullet+}$ [40]. However, polarisation of an ITIES formed between water and butyronitrile using the potential determining BF_4^- anion increased the efficiency of the photoelectrocatalytic OER by enhancing the separation of the photoproducts (protons and TTF) by pumping protons to the aqueous phase [42]. Polarisation at the negative extreme, using the bis(triphenylphosphoranylidine)ammonium cation (BA^+), or positive extreme, using the tetrakis(pentafluorophenylborate) anion (TB^-), of the potential window yielded suboptimal efficiency (Figure 2b(ii)). With BA^+, the $TTF^{\bullet+}$ was extracted to the aqueous phase and the resultant $TTF/TTF^{\bullet+}Cl^-$ assemblies formed were less photocatalytic, while with TB^- a stable "ionosome" emulsion [66] formed that scattered the light. Deposition of the $TTF/TTF^{\bullet+}BF_4^-$ molecular assembly on a carbon electrode in the anodic compartment of a water-splitting H-cell permitted the electrochemical recycling of the electron acceptor $TTF^{\bullet+}$ in a water|butyronitrile emulsion [41]. Girault and co-workers also reported OER at the ITIES simply using photo-excitable fluorinated 7,7,8,8-tetracyanoquinodimethane (F_4TCNQ) aggregates as an electron acceptor [43]. In the proposed mechanism, four photo-excited $TCNQF_4^{\bullet+}$ radical cations stacked in an aggregate oxidise water to release O_2 and four protons, with the latter neutralising the $TCNQF_4^{2-}$ dianions to form H_2TCNQF_4 [43].

Photoelectrocatalysis of the HER at the ITIES has been achieved using organic soluble osmocene [44], decamethylosmocene [45] and decamethylruthenocene [46–49]. Based on their standard redox potentials, none of these metallocenes reduce protons pumped across a positively polarised ITIES spontaneously. However, all act as photo-redox catalysts and evolve H_2 to varying degrees *via* the corresponding hydride species when illuminated. The ability to generate H_2 with weak reductants makes these molecules highly suited for integration into the cathodic compartment of a biphasic H-cell as the oxidised form can be reduced at very positive redox potentials, thereby requiring less electrochemical driving force [67].

Photoelectrocatalysis of the ORR at the ITIES has been achieved by introducing photoactive porphyrin molecules to the aqueous phase [50,51,54] and by assembling either porphyrin-based supramolecular nanostructures [57] or bare [52,55,56] and dye-sensitised [53] colloidal TiO_2 semiconductor NPs at the ITIES. Aqueous soluble porphyrins, for example zinc(II) meso-tetrakis(4-carboxyphenyl)porphyrins (ZnTPPc), act as a photo-redox catalyst at the ITIES. Upon illumination, the excited state is reductively quenched by IET from an organic soluble ferrocene-derivative. The ground state of the porphyrin is then regenerated by binding O_2 and reducing it. Only porphyrins present at the ITIES are photoelectrocatalytically active and therefore the efficiency of the photoelectrocatalytic ORR, as monitored by the magnitude of photocurrent transients recorded at the ITIES, is limited by the interfacial surface coverage of the porphyrin molecules. By optimally tuning the pH of the aqueous phase to match the p*K*a of the carboxyphenyl-substituents on ZnTPPc, Scanlon and co-workers have self-assembled ZnTPPc into films of highly ordered supramolecular nanostructures at a polarisable aqueous|TFT interface (Figure 2c(i) [57,68–70]. Due to the huge increase in interfacial porphyrin surface coverage, the multilayers of interfacial nanostructures are more efficient light harvesters, with the photocurrent due to the photoelectrocatalytic ORR increasing an order of magnitude compared to studies with ZnTPPc simply dissolved in the bulk aqueous phase (Figure 2c(ii)) [57].

Colloidal TiO_2 semiconductor NPs can be electrostatically assembled at ITIES by tuning the aqueous pH and applied $\Delta_o^w\phi$ [52,55]. Upon illumination, O_2 is photoelectrocatalytically reduced by the conduction band electrons of TiO_2, while a ferrocene-derivative is oxidised by interfacial hole-transfer across the ITIES mediated by surface $OH^\bullet$ radicals. Plana et al. developed a methodology involving sonication and the use of relatively high aqueous electrolyte concentrations to prepare thick interfacial films of coalesced TiO_2 NPs at the ITIES [56]. Despite the mesoporous nature of the interfacial TiO_2 film, cyclic voltammograms indicated that the ITIES retained a characteristic molecular sharpness. Using this setup, incident photon-to-current

efficiencies (IPCE) of 75% were reported [56], far beyond the ca. 1% achieved for ITIES modified with sub-monolayer coverages of photoactive porphyrin molecules or TiO_2 NPs. In an early contribution to this field, Fermín et al. demonstrated that photocurrent responses originating from the photoelectrocatalytic OER and associated oxidation of a ferrocene-derivative can be extended into the visible region by dye sensitisation of TiO_2 NPs assembled at the ITIES [53].

Bioelectrocatalysis at the ITIES

Polarised liquid|liquid interfaces provide the required fluidic, amphipathic environment for redox protein adsorption, and can replicate the electrostatic and/or hydrophobic interactions required to mimic the biological membrane [71]. Furthermore, the electric fields of up to 10^9 $V \cdot m^{-1}$ experienced by peripheral membrane proteins are replicated at the ITIES without the need to introduce any solid electrode architectures [72]. In this context, the electrocatalytic activity of the model protein cytochrome *c* (Cyt *c*) towards the ORR has recently been demonstrated at the ITIES [58,59]. Cyclic voltammograms with Cyt *c* in an aqueous phosphate buffer solution and the reductant DcMFc in an organic electrolyte solution show two voltammetric signals, one reversible and the other irreversible (Figure 3a). The irreversible signal at positive potentials is attributed to the electrocatalytic ORR, while the reversible peak at negative potentials is attributed to the ion transfer of $DcMFc^+$ cations produced during O_2 reduction [58]. This bioelectrocatalytic IET reaction was facilitated at positive potentials due to electrostatic and hydrophobic interactions between Cyt *c* and tetrakis(pentafluorophenyl)borate (TB^-) organic electrolyte anions in the mixed solvent region. UV/vis spectroscopy in total internal reflection (TIR-UV/vis) configuration demonstrated that Cyt *c* adsorbs and is partially denatured at a positive applied $\Delta_o^w\phi$ (ca. 0.5 V). In contrast, no adsorbed Cyt *c* species were detected at negative applied $\Delta_o^w\phi$ [58]. These findings were supported by Molecular dynamic (MD) computational modelling, where positive potentials promoted interactions between cationic lysine residues that surround the active site of Cyt *c* and TB^- (Figure 3b). The consequences of these interactions are two-fold: (i) causing a conformational change of the adsorbed Cyt *c* from its native state that exposes the redox-active heme to O_2 and (ii) ensuring the partially exposed heme-pocket is orientated perpendicular to the liquid|liquid interface to favour interfacial electron transfer with DcMFc. The intensity of the irreversible ORR signal decreases with each cycle (Figure 3a) as Cyt *c* becomes progressively more denatured and redox inactive due to its continued interactions with the organic solvent and TB^-. The electrochemical behaviour of Cyt *c* at a positively polarised ITIES mimics Cyt *c*'s *in vivo* peroxidase activity in the inner mitochondrial membrane at the onset of apoptosis in which reactive O_2 species (ROS; such as H_2O_2) are reduced at the heme [58]. Specifically, the dual biological roles of the anionic phospholipid cardiolipin in this process, as a disrupter of the tertiary structure of Cyt *c* and sacrificial oxidant, are played by TB^- and DcMFc, respectively (Figure 3c).

Cyt *c*'s electrocatalytic activity towards the ORR at the ITIES is enhanced in the presence of denaturing agents such as guanidinium chloride (GdmCl) and urea (Figure 3d) [59]. The magnitude of this enhancement is correlated with physicochemical changes to the liquid|liquid interface and, most importantly, conformational changes to the adsorbed Cyt *c* specific to each chaotrope. MD modelling revealed that the distinct Cyt *c* unfolding mechanism with GdmCl leads to a more open heme pocket structure than when urea is added, and thus GdmCl shows a greater enhancement in electrocatalytic activity towards the ORR [59]. Additionally, Gdm^+ cations penetrate the interface, creating a more hydrophobic environment that increases the interfacial concentration of DcMFc in the mixed solvent region and thereby enhances IET. Conversely, urea partially impedes access of the organic solvent to the water phase and hinders IET.

Normalising electrocatalytic performance at the ITIES

As outlined in the previous sections, over the years, many different catalyst materials have been investigated for the HER and ORR at polarised liquid|liquid interfaces. Unfortunately, there has been very little discussion in the field on how to normalise and compare the electrocatalytic performance of different materials at the ITIES. Experiments have been performed in vastly different experimental conditions, with very different catalyst amounts. Also, catalysts may be added as a powder (*e.g.*, [16,27]) or formed *in situ* by reduction from the precursors (*e.g.*, [9,21]). Therefore, to allow better comparison of the results, we believe that stricter standards are required and recently suggested best practises for reporting electrocatalytic performance of nanomaterials should also be applied for electrocatalytic work at the ITIES [73]. One of the recommendations was to report the turnover frequency, but this is challenging to estimate as typically the number of active sites per area is not known. Unlike for catalysts attached on an electrode surface, even estimation of the electrochemically active surface area of catalayst dispersed in solution or attached at the ITIES remains a challenge. As a compromise, we suggest at least normalising the reaction rates by the mass or the molar amount of the catalyst. As an example, we have analysed the data on the biphasic HER presented in the literature in so-called "shake-flask experiments" (Figure 4). The latter involved DcMFc dissolved in a 1,2-dichloroethane phase reacting under stirring with protons transferred to the

Figure 3

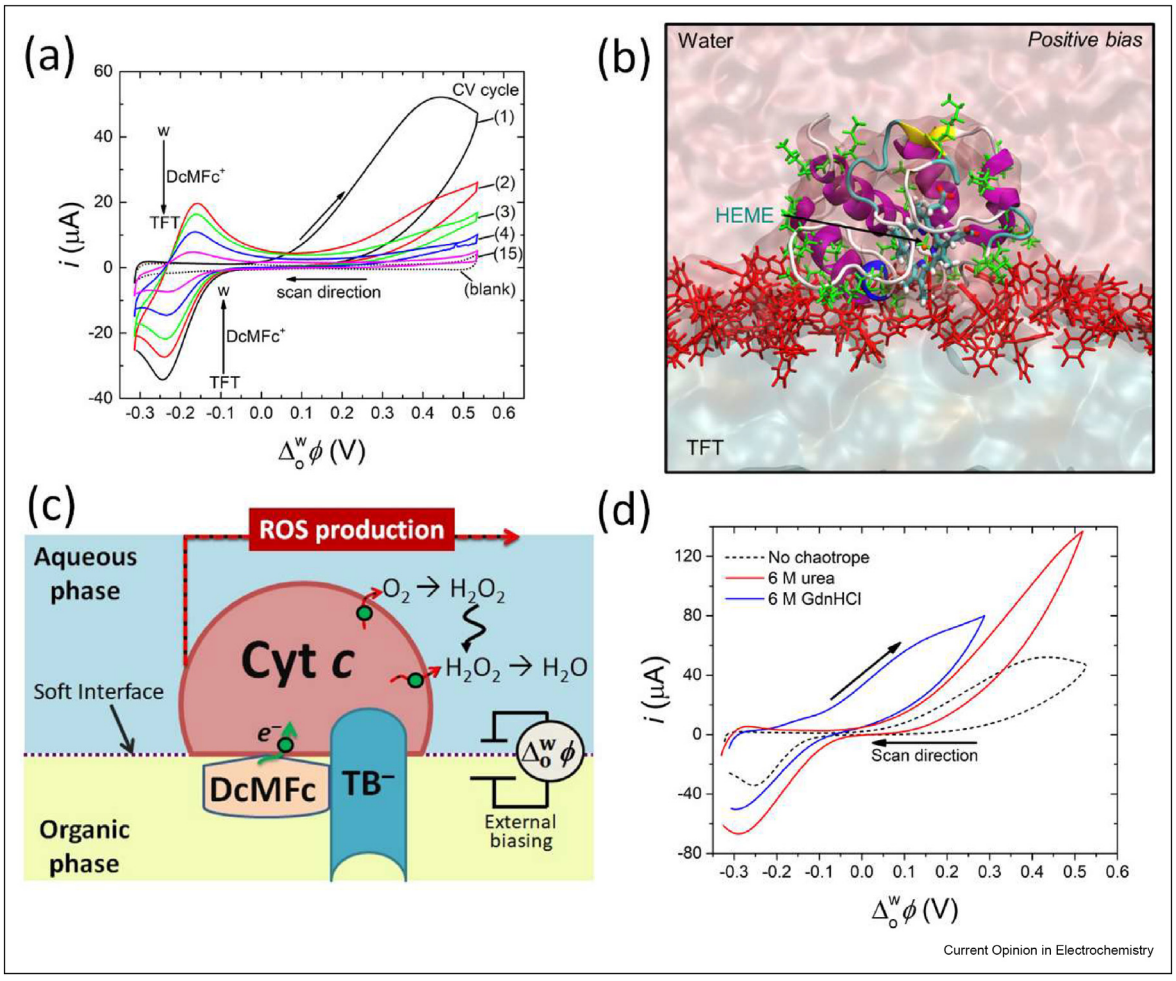

Bioelectrocatalysis at the ITIES. (a) Cyclic voltammetry with 10 μM Cyt *c* in a phosphate buffer solution (60 mM Na_2HPO_4 and 20 mM KH_2PO_4 at pH 7) and 500 μM DcMFc in a solution of 5 mM bis(triphenylphosphoranylidene)ammonium tetrakis(pentafluorophenyl)borate (BATB) organic electrolyte in TFT under aerobic conditions. The scan rate used was 20 mV s^{-1}. **(b)** Representative molecular dynamics snapshots showing the orientation of the Cyt *c* heme active site at a positively polarised liquid|liquid interface. The Lys residues on the surface of Cyt *c* are shown as green ball and sticks, while the BA^+ and TB^- ions from the electrolyte in the TFT organic phase are shown as blue and red ball and sticks, respectively. **(c)** Schematic of the biomimetic electrified aqueous|organic interface at which DcMFc and TB^- anions activate Cyt *c* for reduction of reactive O_2 species. The electrons are represented by green circles. **(d)** Cyclic voltammetry of 10 μM Cyt *c* and 1 mM DcMFc under aerobic conditions, as described in part **(a)**, with and without 6 M urea or GdmCl. The scan rate was 20 mV s^{-1}. **(a)**, **(b)** and **(c)** are reproduced with permission from ref. [58]. Copyright 2021 American Association for the Advancement of Science (AAAS). **(d)** is reproduced from ref. [59] with permission from the Royal Society of Chemistry. Copyright 2022. (For interpretation of the references to colour in this figure legend, the reader is referred to the Web version of this article.)

aqueous phase after positive polarisation of the liquid-|liquid interface by distribution of lithium tetrakis(-pentafluorophenyl)borate (LiTB; initially dissolved in the organic phase) between the phases.

For analysis of the data extracted from the literature [9,16–19,21,31,32,34], we have assumed that first-order kinetics with respect to the DcMFc concentration is followed initially, and the catalyst affects the rate constant of the reaction. This assumption is not strictly true, as some of the catalysts have shown different kinetics [18], but it serves as a first approximation. Apparent first-order reaction rate constants (unit of 1/s) have been extracted for all the catalysts and in the absence of a catalyst (Figure 4a), and the rate constants have been normalised by the mass of the metal (mg/L; Figure 4b), or the concentration of the catalyst (mmol/L; Figure 4c) and divided into catalysts deposited on high-surface-area carbon, as nanomaterials, as catalysts formed by electrodeposition and as microparticles.

The reaction rates depend on the number of active sites, so nanostructuring of the catalysts leads to enhanced normalised reaction rates. Additionally, deposition of the

Figure 4

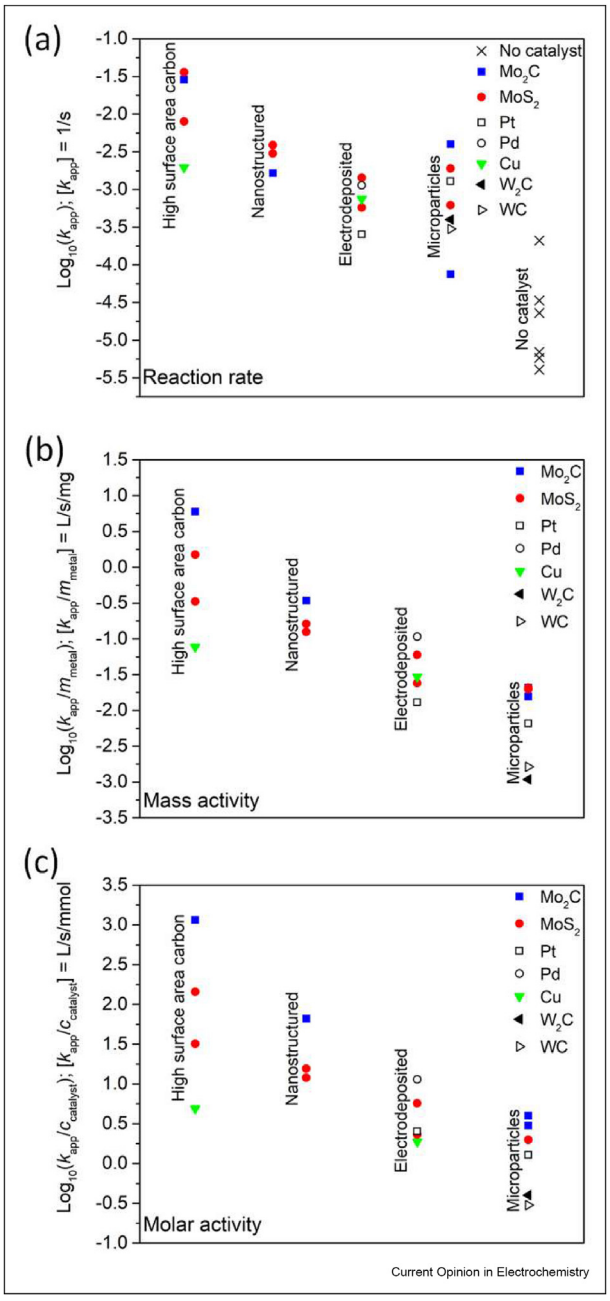

Normalising electrocatalytic performance at the ITIES. (a) Apparent first-order reaction rate constants (k_{app} with a unit of 1/s) extracted in the absence and presence of the catalysts Mo_2C, MoS_2, metallic (Pt, Pd and Cu) nanoparticles, W_2C and WC, either deposited on high-surface-area carbon, as nanomaterials, as catalysts formed by electrodeposition, or as microparticles. The rate constants were normalised **(b)** by the mass (mg/L) of the metal (k_{app}/m_{metal} with a unit of L/s/mg) and **(c)** the concentration (mmol/L) of the active catalyst ($k_{app}/c_{catalyst}$ with a unit of L/s/mmol). The data was extracted from references [9,16–19,21,31,32,34] and is available on Zenodo (https://doi.org/10.5281/zenodo.7400926) to download.

catalyst on a high-surface-area carbon leads to the highest normalised rates. This is because both hydrogen evolution and DcMFc oxidation need to take place at the redox electrocatalyst at the same rate. The overpotential for each reaction depends on the area available for the reactions, as explained in a recent review [8]. For supported catalysts, the area available for DcMFc oxidation taking place at the support is much higher than for the HER taking place mostly at the catalyst. For unsupported particles, the areas available for both reactions can be considered similar. Therefore, the driving force will be higher on the supported catalysts, leading to higher rates.

Analysis of only the reaction rates can lead to misinterpretation of the activities. For example, Mo_2C microparticles show very different reaction rates because the catalyst concentration varied between 25 μM and 1 mM, but this difference disappears when the activities are normalised either by catalyst mass or concentration. Concentration normalised data shows slightly higher activity for Mo_2C than for MoS_2 while the difference is smaller for metal mass normalised data, as the carbide contains twice the mass of the metal.

The data also shows high variability in the reaction rates measured in the absence of catalyst. This might indicate that some chemicals, flasks or even stir bars [74] may very easily cause contamination. Therefore, the practise to compare acceleration to the uncatalysed reaction can lead to inaccurate conclusions. We highlight that carefully cleaned glassware and stir bars should be used for these experiments.

Conclusions and outlook

The diversity of reactions electrocatalysed at the ITIES remains low, with the overwhelming majority of studies pertaining to the HER and ORR, followed by more challenging OER studies [60]. Scope clearly exists to electrocatalyse other reactions that may benefit from a biphasic environment, as shown by the electrocatalytic oxidation of S_8 [35], or lead to the direct electrosynthesis of thin films of nanocomposites (encompassing the interfacial electrocatalyst), as shown by the electrocatalytic oxidation of DMcT by AuNPs [36]. A particularly important reaction that is conspicuous by its absence in the literature is the carbon dioxide reduction reaction (CO_2RR) at the ITIES. A key challenge limiting the efficiency of the (photo)electrochemical CO_2RR is the low solubility of CO_2 in water at standard conditions (~35 mM). However, organic solvents permit higher CO_2 solubility and enable different reaction products, including value-added C_2+ hydrocarbons like oxalate [75]. Furthermore, aprotic organic solvents eliminate the competing HER, an arduous task in aqueous electrolytes [76]. Thus, biphasic systems may simultaneously harness desirable attributes of both the aqueous phase (proton source) and organic phase (inhibit H_2 evolution, increase access to C_2+ hydrocarbons, reservoir of CO_2) towards the CO_2RR. To date,

biphasic CO_2RR systems have been studied using water-miscible organic solvents, *e.g.*, acetonitrile [75,77], immiscible aqueous|organic emulsions [78] and supercritical CO_2|ionic liquid biphasic systems [79–81]. However, the benefits of polarisation of an ITIES to drive the biphasic (photo)electrochemical CO_2RR towards selective C_2+ hydrocarbon production have never been explored. Additionally, nitrogen reduction reactions should also be explored [82].

SECM is a powerful methodology to probe the redox kinetics of any (photo)electrocatalyst as a function of the applied $\Delta_o^w\phi$, as clearly demonstrated by the series of articles by Rastgar et al. to photoelectrocatalyse the OER by an interfacial film of $BiVO_4$ [37–39]. Thus, the further development of SECM as a key methodology to combine with (photo)electrocatalysis at the ITIES will allow the measurement of the "true" (photo)electrocatalytic activity of specific materials without interfering effects arising from interactions of the (photo)electrocatalyst with an underlying solid electrode surface, *e.g.*, contact resistance [8].

The field of bioelectrocatalysis at the ITIES is still in its infancy. Thus, studies with proteins beyond the model Cyt *c* system, such as oxidases [83] and dehydrogenases [84], are required to clarify the limitations and advantages of this new research topic. Furthermore, major scope exists to modify the liquid|liquid interface with phospholipid monolayers to enhance the biocompatibility of the ITIES and optimise IET with proteins. Electrochemical activation of a proteins' enzymatic activities at the ITIES will open exciting new avenues to realise biofuel cell and artificial photosynthesis-based energy conversion and storage, drug screening for medical applications, and (bio)sensing.

Two-phase shake flask methods offer a quick and simple method to test the activity of powdered catalysts for different reactions. For a more careful comparison of the catalysts, the active surface area should be known. For supported catalysts, the loading of the catalyst will also have a significant effect on the measured rates. Additionally, methods to evaluate the stability of the catalysts should be developed, for example, based on electrochemical setups [67].

Declaration of competing interest

The authors declare that they have no known competing financial interests or personal relationships that could have appeared to influence the work reported in this paper.

Data availability

The data extracted from references [9,16–19,21,31,32,34] to prepare Figure 4 is available on Zenodo (https://doi.org/10.5281/zenodo.7400926) to download.

Acknowledgments

M.D.S. acknowledges funding from the European Research Council through a Starting Grant (agreement no. 716792). A.G.-Q. acknowledges funding received from an Irish Research Council (IRC) Government of Ireland Postdoctoral Fellowship Award (grant no. GOIPD/2018/252) and a Marie Skłodowska-Curie Postdoctoral Fellowship (grant no. MSCA-IF-EF-ST 2020/101018277). P.P. acknowledges funding from the European Research Council through a Starting Grant (agreement no. 950038), the Academy Research Fellow funding and project funding by the Academy of Finland (Grants No. 315739 and 334828).

References

Papers of particular interest, published within the period of review, have been highlighted as:

* of special interest
** of outstanding interest

1. Mendez MA, Partovi-Nia R, Hatay I, Su B, Ge P, Olaya A, Younan N, Hojeij M, Girault HH: **Molecular electrocatalysis at soft interfaces**. *Phys Chem Chem Phys* 2010, **12**:15163–15171, https://doi.org/10.1039/c0cp00590h.

2. Rodgers ANJ, Booth SG, Dryfe RAW: **Particle deposition and catalysis at the interface between two immiscible electrolyte solutions (ITIES): a mini-review**. *Electrochem Commun* 2014, **47**:17–20, https://doi.org/10.1016/j.elecom.2014.07.009.

3. Booth SG, Dryfe RAW: **Assembly of nanoscale objects at the liquid/liquid interface**. *J Phys Chem C* 2015, **119**:23295–23309, https://doi.org/10.1021/acs.jpcc.5b07733.

4. Poltorak L, Gamero-Quijano A, Herzog G, Walcarius A: **Decorating soft electrified interfaces: from molecular assemblies to nano-objects**. *Appl Mater Today* 2017, **9**:533–550, https://doi.org/10.1016/j.apmt.2017.10.001.

5. Scanlon MD, Smirnov E, Stockmann TJ, Peljo P: **Gold nanofilms at liquid-liquid interfaces: an emerging platform for redox electrocatalysis, nanoplasmonic sensors, and electrovariable optics**. *Chem Rev* 2018, **118**:3722–3751, https://doi.org/10.1021/acs.chemrev.7b00595.

6. Zarbin AJGG: **Liquid–liquid interfaces: a unique and advantageous environment to prepare and process thin films of complex materials**. *Mater Horiz* 2021, **8**:1409–1432, https://doi.org/10.1039/D0MH01676D.

7. Zhao J, Jiang C, Liu Y: **Nanomaterials at interfaces between immiscible electrolyte solutions**. *Aust J Chem* 2020, **73**:861–867, https://doi.org/10.1071/CH19532.

8. Peljo P, Scanlon MD, Olaya AJ, Rivier L, Smirnov E, Girault HH: **Redox electrocatalysis of floating nanoparticles: determining electrocatalytic properties without the influence of solid supports**. *J Phys Chem Lett* 2017, **8**:3564–3575, https://doi.org/10.1021/acs.jpclett.7b00685.

9. Nieminen JJ, Hatay I, Ge P, Mendez MA, Murtomäki L, Girault HH: **Hydrogen evolution catalyzed by electrodeposited nanoparticles at the liquid/liquid interface**. *Chem Commun* 2011, **47**:5548–5550, https://doi.org/10.1039/C1CC10637F.

10. Gründer Y, Fabian MD, Booth SG, Plana D, Fermín DJ, Hill PI, Dryfe RAW: **Solids at the liquid–liquid interface: electrocatalysis with pre-formed nanoparticles**. *Electrochim Acta* 2013, **110**:809–815, https://doi.org/10.1016/j.electacta.2013.03.185.

11. Rastgar S, Deng H, Cortés-Salazar F, Scanlon MD, Pribil M, Amstutz V, Karyakin AA, Shahrokhian S, Girault HH: **Oxygen reduction at soft interfaces catalyzed by in situ-generated reduced graphene oxide**. *Chemelectrochem* 2014, **1**:59–63, https://doi.org/10.1002/celc.201300140.

12. Smirnov E, Peljo P, Scanlon MD, Girault HH: **Gold nanofilm redox catalysis for oxygen reduction at soft interfaces**. *Electrochim Acta* 2016, **197**:362–373, https://doi.org/10.1016/j.electacta.2015.10.104.

13. Rodgers ANJ, Dryfe RAW: **Oxygen reduction at the liquid-liquid interface: bipolar electrochemistry through adsorbed graphene layers**. *Chemelectrochem* 2016, **3**:472–479, https://doi.org/10.1002/celc.201500343.

14. Stockmann TJ, Angelé L, Brasiliense V, Combellas C, Kanoufi F: **Platinum nanoparticle impacts at a liquid|liquid interface**. *Angew Chem* 2017, **129**:13678–13682, https://doi.org/10.1002/ange.201707589.

** This study is the first to combine the concepts of electrocatalysis at the ITIES and nanoparticle impact studies. Current spikes were recorded at a micron-sized ITIES due to the electrocatalytic ORR upon impact of Pt NPs at the polarised liquid|liquid interface with ferrocene acting as the electron donor.

15. Warczak M, Osial M, Urbanska W, Pisarek M, Nogala W, Opallo M: **Hydrogen peroxide generation catalyzed by battery waste material, Electrochem**. *Commun Now* 2022, **136**, 107239, https://doi.org/10.1016/j.elecom.2022.107239.

16. Hatay I, Ge PY, Vrubel H, Hu X, Girault HH: **Hydrogen evolution at polarised liquid|liquid interfaces catalyzed by molybdenum disulfide**. *Energy Environ Sci* 2011, **4**:4246, https://doi.org/10.1039/c1ee01996a.

* This is the first reported example of an inorganic material, molybdenum disulfide (MoS_2), being used to electrocatalyse the HER at the ITIES.

17. Ge P, Scanlon MD, Peljo P, Bian X, Vubrel H, O'neill A, Coleman JN, Cantoni M, Hu X, Kontturi K, Liu BH, Girault HH: **Hydrogen evolution across nano-Schottky junctions at carbon supported MoS_2 catalysts in biphasic liquid systems**. *Chem Commun* 2012, **48**:6484–6486, https://doi.org/10.1039/c2cc31398g.

18. Scanlon MD, Bian X, Vrubel H, Amstutz V, Schenk K, Hu X, Liu B, Girault HH: **Low-cost industrially available molybdenum boride and carbide as "platinum-like" catalysts for the hydrogen evolution reaction in biphasic liquid systems**. *Phys Chem Chem Phys* 2013, **15**:2847, https://doi.org/10.1039/c2cp44522k.

19. Bian X, Scanlon MD, Wang S, Liao L, Tang Y, Liu B, Girault HH: **Floating conductive catalytic nano-rafts at soft interfaces for hydrogen evolution**. *Chem Sci* 2013, **4**:3432–3441, https://doi.org/10.1039/c3sc51290h.

20. Aslan E, Hatay Patir I, Ersoz M: **Catalytic hydrogen evolution by tungsten disulfide at liquid-liquid interfaces**. *ChemCatChem* 2014, **6**:2832–2835, https://doi.org/10.1002/cctc.201402473.

21. Aslan E, Patir IH, Ersoz M: **Cu nanoparticles electrodeposited at liquid-liquid interfaces: a highly efficient catalyst for the hydrogen evolution reaction**. *Chem Eur J* 2015, **21**:4585–4589, https://doi.org/10.1002/chem.201406615.

22. Ozel F, Yar A, Aslan E, Arkan E, Aljabour A, Can M, Patir IH, Kus M, Ersoz M: **Earth-abundant Cu_2CoSnS_4 nanofibers for highly efficient H_2 evolution at soft interfaces**. *ChemNanoMat* 2015, **1**:477–481, https://doi.org/10.1002/cnma.201500113.

23. Ozel F, Aslan E, Sarilmaz A, Hatay Patir I: **Hydrogen evolution catalyzed by Cu_2WS_4 at liquid–liquid interfaces**. *ACS Appl Mater Interfaces* 2016, **8**:25881–25887, https://doi.org/10.1021/acsami.6b05582.

24. Aslan E, Akin I, Patir IH: **Highly active cobalt sulfide/carbon nanotube catalyst for hydrogen evolution at soft interfaces**. *Chem Eur J* 2016, **22**:5342–5349, https://doi.org/10.1002/chem.201505048.

25. Aslan E, Akin I, Patir IH: **Enhanced hydrogen evolution catalysis based on Cu nanoparticles deposited on carbon nanotubes at the liquid/liquid interface**. *ChemCatChem* 2016, **8**:719–723, https://doi.org/10.1002/cctc.201501119.

26. Akin I, Aslan E, Hatay Patir I: **Enhanced hydrogen evolution catalysis at the liquid/liquid interface by Ni_xS_y and Ni_xS_y/carbon nanotube catalysts**. *Eur J Inorg Chem* 2017, **2017**:3961–3966, https://doi.org/10.1002/ejic.201700873.

27. Hirunpinyopas W, Rodgers ANJ, Worrall SD, Bissett MA, Dryfe RAW: **Hydrogen evolution at liquid|liquid interfaces catalyzed by 2D materials**. *ChemNanoMat* 2017, **3**:428–435, https://doi.org/10.1002/cnma.201700047.

28. Aslan E, Sarilmaz A, Ozel F, Hatay Patir I, Girault HH: **Catalytic hydrogen evolution by molybdenum-based ternary metal sulfide nanoparticles**. *ACS Appl Nano Mater* 2019, **2**:7204–7213, https://doi.org/10.1021/acsanm.9b01694.

29. Aslan E, Sarilmaz A, Ozel F, Hatay Patir I, Girault HH: **1D amorphous tungsten-based ternary refractory metal sulfides for catalytic hydrogen evolution at soft interfaces**. *ChemNanoMat* 2019, **5**:1461–1466, https://doi.org/10.1002/cnma.201900536.

30. Aslan E, Sarilmaz A, Yanalak G, Ozel SS, Ozel F, Patir IH: **Transition metal–incorporated tungsten-based ternary refractory metal selenides ($MWSe_x$; M = Fe, Co, Ni, and Mn) as hydrogen evolution catalysts at soft interfaces**. *Mater Today Energy* 2020, **18**, 100510, https://doi.org/10.1016/j.mtener.2020.100510.

31. Aslan E, Yanalak G, Hatay Patir I: **Enhanced hydrogen evolution reaction catalysis at template-free liquid/liquid interfaces by *in situ* electrodeposited amorphous molybdenum sulfide on carbon nanotubes**. *ACS Appl Energy Mater* 2021, **4**:8330–8339, https://doi.org/10.1021/acsaem.1c01554.

32. Aslan E, Patir IH: **Catalysis of hydrogen evolution reaction by in situ electrodeposited amorphous molybdenum sulfide at soft interfaces**. *Mater Today Energy* 2021, **21**, 100742, https://doi.org/10.1016/j.mtener.2021.100742.

33. Aslan E, Eroğlu Z, Yanalak G, Metin Ö, Hatay Patir I: **Enhanced hydrogen evolution via in situ generated 2D black phosphorous nanocomposites at the liquid/liquid interfaces**. *Appl Surf Sci* 2022, **604**, 154435, https://doi.org/10.1016/j.apsusc.2022.154435.

34. Aslan E, Hatay Patir I: **In situ copper nanoparticles on reduced graphene oxide (rGO/Cu) for biphasic hydrogen evolution**. *Chemelectrochem* 2022, **9**, https://doi.org/10.1002/celc.202200381.

35. Suárez-Herrera MF, Gamero-Quijano A, Solla-Gullón J, Scanlon MD: **Mimicking the microbial oxidation of elemental sulfur with a biphasic electrochemical cell**. *Electrochim Acta* 2022, **401**, 139443, https://doi.org/10.1016/j.electacta.2021.139443.

** This is a rare example of a film of AuNPs at the ITIES being used to electrocatalyse a reaction besides the HER and ORR. In this case, the metallic interfacial electrocatalyst is used to oxidise elemental sulfur (S_8) under aerobic conditions.

36. Suárez-Herrera MF, Gamero-Quijano A, Scanlon MD: **Electrosynthesis of poly(2,5-dimercapto-1,3,4-thiadiazole) films and their composites with gold nanoparticles at a polarised liquid|liquid interface**. *Electrochim Acta* 2022, **424**, 140677, https://doi.org/10.1016/j.electacta.2022.140677.

37. Rastgar S, Pilarski M, Wittstock G: **A polarized liquid-liquid interface meets visible light-driven catalytic water oxidation**. *Chem Commun* 2016, **52**:11382–11385, https://doi.org/10.1039/c6cc04275a.

* This study is the first example of the photoelectrocatalysis of the OER at the ITIES using an interfacial film of $BiVO_4$ photocatalyst and $[Co(bpy)_3](PF_6)_3$ as both the sacrificial oxidant and a SECM probe.

38. Rastgar S, Wittstock G: **Characterization of photoactivity of nanostructured $BiVO_4$ at polarized liquid–liquid interfaces by scanning electrochemical microscopy**. *J Phys Chem C* 2017, **121**:25941–25948, https://doi.org/10.1021/acs.jpcc.7b09550.

** Using SECM feedback approach curves, the kinetics of the photoelectrocatalytic OER at the ITIES were shown to increase as the applied $\Delta_o^w\phi$ shifted to less positive potentials by varying the concentration ratio of a potential determining anion (ClO_4^-) in each phase.

39. Rastgar S, Wittstock G: **In situ microtitration of intermediates of water oxidation reaction at nanoparticles assembled at water/oil interfaces**. *J Phys Chem C* 2018, **122**:12963–12969, https://doi.org/10.1021/acs.jpcc.8b03745.

40. Olaya AJ, Omatsu T, Hidalgo-Acosta JC, Riva JS, Bassetto VC, Gasilova N, Girault HH: **A self-assembled organic/metal junction for water photo-oxidation**. *J Am Chem Soc* 2019, **141**:6765–6774, https://doi.org/10.1021/jacs.9b02693.

* In this article, *in situ* self-assembled *p*-type semiconductors, consisting of tetrathiafulvalene (TTF), $TTF^{\bullet+}$ and BF_4^- or PF_6^- molecular assemblies adsorbed on the surface of Co_3O_4 or Pt nanoparticles, are introduced as an electron acceptor/photosensitiser redox OER photoelectrocatalyst suitable for use in a biphasic system.

41. Olaya AJ, Riva JS, Baster D, Silva WO, Pichard F, Girault HH: **Visible-light-driven water oxidation on self-assembled metal-free Organic@Carbon junctions at neutral pH**. *JACS Au* 2021, **1**:2294–2302, https://doi.org/10.1021/jacsau.1c00408.

42. ** Riva JS, Girault HH, Olaya AJ: **Water photo-oxidation on self-assembled organic/Co_3O_4 metal junctions in biphasic systems**. *Electrochim Acta* 2022, **414**, 140166, https://doi.org/10.1016/j.electacta.2022.140166.
In this study, polarisation of an ITIES formed between water and butyronitrile using the potential determining BF_4^- anion was shown to increase the efficiency of the photoelectrocatalytic OER using TTF/$TTF^{\bullet+}$ BF_4^- adsorbed on the surface of Co_3O_4 or Pt nanoparticles as the interfacial photocatalyst. Polarisation of the ITIES aided separation of the photoproducts (protons and TTF) by pumping protons to the aqueous phase.

43. * Moya Betancourt SN, Riva JS, Uranga JG, Olaya AJ, Girault HH: **Visible-light driven water oxidation and oxygen production at soft interfaces**. *Chem Commun* 2022, **58**:3965–3968, https://doi.org/10.1039/D1CC07013D.
In this article, OER at the ITIES is achieved by simply using photo-excitable F_4TCNQ aggregates as an electron acceptor, without any metal, metal oxide or molecular catalyst.

44. Ge P, Todorova TK, Patir IH, Olaya AJ, Vrubel H, Mendez MA, Hu X, Corminboeuf C, Girault HH: **Biphasic water splitting by osmocene**. *Proc Natl Acad Sci USA* 2012, **109**:11558–11563, https://doi.org/10.1073/pnas.1203743109.

45. Ge P, Olaya AJ, Scanlon MD, Hatay Patir I, Vrubel H, Girault HH: **Photoinduced biphasic hydrogen evolution: decamethylosmocene as a light-driven electron donor**. *ChemPhysChem* 2013, **14**:2308–2316, https://doi.org/10.1002/cphc.201300122.

46. Rivier L, Stockmann TJ, Mendez MA, Scanlon MD, Peljo P, Opallo M, Girault HH: **Decamethylruthenocene hydride and hydrogen formation at Liquid|Liquid interfaces**. *J Phys Chem C* 2015, **119**:25761–25769, https://doi.org/10.1021/acs.jpcc.5b08148.

47. Rivier L, Peljo P, Vannay LAC, Gschwend GC, Mendez MA, Corminboeuf C, Scanlon MD, Girault HH: **Photoproduction of hydrogen by decamethylruthenocene combined with electrochemical recycling**. *Angew Chem Int Ed* 2017, **56**:2324–2327, https://doi.org/10.1002/anie.201610240.

48. Jedraszko J, Adamiak W, Nogala W, Girault HH, Opallo M: **SECM study of hydrogen photogeneration in a 1,2-dichloroethane | water biphasic system with decamethylruthenocene electron donor regeneration**. *J Electroanal Chem* 2018, **819**:101–106, https://doi.org/10.1016/j.jelechem.2017.09.026.

49. Rivier L, Peljo P, Maye S, Mendez MA, Vrubel H, Vannay LAC, Corminboeuf C, Scanlon MD, Girault HH: **Mechanistic study on the photogeneration of hydrogen by decamethylruthenocene**. *Chem Eur J* 2019, **25**:12769–12779, https://doi.org/10.1002/chem.201902353.

50. Fermín DJ, Ding Z, Duong HD, Brevet P-F, Girault HH: **Photoinduced electron transfer at liquid/liquid interfaces. 1. Photocurrent measurements associated with heterogeneous quenching of zinc porphyrins**. *J Phys Chem B* 1998, **102**:10334–10341, https://doi.org/10.1021/jp983196m.

51. Fermín DJ, Duong HD, Ding Z, Brevet P-F, Girault HH: **Photoinduced electron transfer at liquid/liquid interfaces. Part III. Photoelectrochemical responses involving porphyrin ion pairs**. *J Am Chem Soc* 1999, **121**:10203–10210, https://doi.org/10.1021/ja992215i.

52. Jensen H, Fermín DJ, Moser JE, Girault HH: **Organization and reactivity of nanoparticles at molecular interfaces. Part I. Photoelectrochemical responses involving TiO_2 nanoparticles assembled at polarizable water|1,2-dichloroethane junctions**. *J Phys Chem B* 2002, **106**:10908–10914, https://doi.org/10.1021/jp0261253.

53. Fermín DJ, Jensen H, Moser JE, Girault HH: **Organisation and reactivity of nanoparticles at molecular interfaces. Part II. Dye sensitisation of TiO_2 nanoparticles assembled at the water|1,2-dichloroethane interface**. *ChemPhysChem* 2003, **4**:85–89, https://doi.org/10.1002/cphc.200390013.

54. Fermín D, Eugster N: **Organisation and photoelectrochemical reactivity of water-soluble metalloporphyrins at the liquid/liquid interface**. In *N4-Macrocycl. Met. Complexes*. Edited by Zagal JH, Bedioui F, Dodelet J-P, New York, NY: Springer New York; 2006:517–574, https://doi.org/10.1007/978-0-387-28430-9_11.

55. Plana D, Fermín DJ: **Photoelectrochemical activity of colloidal TiO_2 nanostructures assembled at polarisable liquid/liquid interfaces**. *J Electroanal Chem* 2016, **780**:373–378, https://doi.org/10.1016/j.jelechem.2015.09.030.

56. * Plana D, Bradley KA, Tiwari D, Fermín DJ: **Over 75% incident-photon-to-current efficiency without solid electrodes**. *Phys Chem Chem Phys* 2016, **18**:12428–12433, https://doi.org/10.1039/C6CP02231F.
In this article, thick interfacial films of coalesced TiO_2 NPs were prepared at the ITIES, yet the ITIES retained a characteristic molecular sharpness. Consequently, an IPCE of 75% was reported, far beyond the ca. 1% achieved for ITIES modified with sub-monolayer coverages of photoactive porphyrin molecules or TiO_2 NPs.

57. * Molina-Osorio AF, Cheung D, O'Dwyer C, Stewart AA, Dossot M, Herzog G, Scanlon MD: **Self-assembly of porphyrin nanostructures at the interface between two immiscible liquids**. *J Phys Chem C* 2020, **124**:6929–6937, https://doi.org/10.1021/acs.jpcc.0c00437.
In this study, by increasing the interfacial surface concentration of the porphyrin through the assembly of a film of ZnTPPc interfacial nanostructures, photocurrents due to the photoelectrocatalytic ORR increasing an order of magnitude compared to studies with ZnTPPc simply dissolved in the bulk aqueous phase

58. ** Gamero-Quijano A, Bhattacharya S, Cazade P-A, Molina-Osorio AF, Beecher C, Djeghader A, Soulimane T, Dossot M, Thompson D, Herzog G, Scanlon MD: **Modulating the pro-apoptotic activity of cytochrome c at a biomimetic electrified interface**. *Sci Adv* 2021, **7**, https://doi.org/10.1126/sciadv.abg411. eabg4119.
This is the first article to demonstrate bioelectrocatalysis at the ITIES, specifically Cyt *c* exhibits electrocatalytic activity towards the ORR. This mimics Cyt *c*'s *in vivo* peroxidase activity in the inner mitochondrial membrane at the onset of apoptosis in which reactive O_2 species (ROS; such as H_2O_2) are reduced at the heme.

59. ** Gamero-Quijano A, Cazade P-A, Bhattacharya S, Walsh S, Herzog G, Thompson D, Scanlon MD: **On the origin of chaotrope-modulated electrocatalytic activity of cytochrome *c* at electrified aqueous|organic interfaces**. *Chem Commun* 2022, **58**:3270–3273, https://doi.org/10.1039/D1CC05293D.
In this article, denaturing agents such as guanidinium chloride and urea are shown to enhance Cyt *c*'s electrocatalytic activity towards the ORR at the ITIES due to physicochemical changes to the liquid|liquid interface and, in particular, conformational changes to the adsorbed Cyt *c* specific to each chaotrope.

60. Opallo M, Dusilo K, Warczak M, Kalisz J: **Hydrogen evolution, oxygen evolution, and oxygen reduction at polarizable Liquid|Liquid interfaces**. *Chemelectrochem* 2022, **9**, e202200513, https://doi.org/10.1002/celc.202200513.

61. Scanlon MD, Peljo P, Mendez MA, Smirnov E, Girault HH: **Charging and discharging at the nanoscale: Fermi level equilibration of metallic nanoparticles**. *Chem Sci* 2015, **6**:2705–2720, https://doi.org/10.1039/c5sc00461f.

62. ** Smirnov E, Peljo P, Scanlon MD, Girault HH: **Interfacial redox catalysis on gold nanofilms at soft interfaces**. *ACS Nano* 2015, **9**:6565–6575, https://doi.org/10.1021/acsnano.5b02547.
This article experimentally demonstrates the concept of an interfacial film of conducting AuNPs acting as a bipolar electrode at the ITIES and, due to Fermi level equilibration, catalytically enhancing the kinetics of electron transfer between redox couples on either side of the liquid|liquid interface.

63. Sokolov SV, Eloul S, Kätelhön E, Batchelor-McAuley C, Compton RG: **Electrode–particle impacts: a users guide**. *Phys Chem Chem Phys* 2017, **19**:28–43, https://doi.org/10.1039/C6CP07788A.

64. Baker LA: **Perspective and prospectus on single-entity electrochemistry**. *J Am Chem Soc* 2018, **140**:15549–15559, https://doi.org/10.1021/jacs.8b09747.

65. Laborda E, Molina A: **Impact experiments at the interface between two immiscible electrolyte solutions (ITIES)**. *Curr. Opin. Electrochem.* 2021, **26**, 100664, https://doi.org/10.1016/j.coelec.2020.100664.

66. Deng H, Peljo P, Huang X, Smirnov E, Sarkar S, Maye S, Girault HH, Mandler D: **Ionosomes: observation of ionic bilayer water clusters**. *J Am Chem Soc* 2021, **143**:7671–7680, https://doi.org/10.1021/jacs.0c12250.

67. Scanlon MD, Peljo P, Rivier L, Vrubel H, Girault HH: **Mediated water electrolysis in biphasic systems**. *Phys Chem Chem Phys* 2017, **19**:22700–22710, https://doi.org/10.1039/C7CP04601D.

68. Molina-Osorio AF, Manzanares JA, Gamero-Quijano A, Scanlon MD: **Electrochemically controlled ion dynamics in porphyrin nanostructures**. *J Phys Chem C* 2020, **124**:18346–18355, https://doi.org/10.1021/acs.jpcc.0c04976.

69. Molina-Osorio AF, Yamamoto S, Robayo-Molina I, Gamero-Quijano A, Nagatani H, Scanlon MD: **A soft on/off switch based on the electrochemically reversible H–J interconversion of a floating porphyrin membrane**. *Chem Sci* 2021, **12**:10227–10232, https://doi.org/10.1039/D0SC05786J.

70. Robayo-Molina I, Molina-Osorio AF, Guinane L, Tofail SAM, Scanlon MD: **Pathway complexity in supramolecular porphyrin self-assembly at an immiscible liquid–liquid interface**. *J Am Chem Soc* 2021, **143**:9060, https://doi.org/10.1021/jacs.1c02481. –9069.

71. Santos HA, García-Morales V, Pereira CM: **Electrochemical properties of phospholipid monolayers at liquid–liquid interfaces**. *ChemPhysChem* 2010, **11**:28–41, https://doi.org/10.1002/cphc.200900609.

72. Hou B, Laanait N, Yu H, Bu W, Yoon J, Lin B, Meron M, Luo G, Vanysek P, Schlossman ML: **Ion distributions at the water/1,2-dichloroethane interface: potential of mean force approach to analyzing X-ray reflectivity and interfacial tension measurements**. *J Phys Chem B* 2013, **117**:5365–5378, https://doi.org/10.1021/jp401892y.

73. Voiry D, Chhowalla M, Gogotsi Y, Kotov NA, Li Y, Penner RM, Schaak RE, Weiss PS: **Best practices for reporting electrocatalytic performance of nanomaterials**. *ACS Nano* 2018, **12**:9635–9638, https://doi.org/10.1021/acsnano.8b07700.

74. Pentsak EO, Eremin DB, Gordeev EG, Ananikov VP: **Phantom reactivity in organic and catalytic reactions as a consequence of microscale destruction and contamination-trapping effects of magnetic stir bars**. *ACS Catal* 2019, **9**:3070–3081, https://doi.org/10.1021/acscatal.9b00294.

75. Fischer J, Lehmann Th, Heitz E: **The production of oxalic acid from CO_2 and H_2O**. *J Appl Electrochem* 1981, **11**:743–750, https://doi.org/10.1007/BF00615179.

76. Moura de Salles Pupo M, Kortlever R: **Electrolyte effects on the electrochemical reduction of CO_2**. *ChemPhysChem* 2019, **20**:2926–2935, https://doi.org/10.1002/cphc.201900680.

77. Díaz-Duque Á, Sandoval-Rojas AP, Molina-Osorio AF, Feliu JM, Suárez-Herrera MF: **Electrochemical reduction of CO_2 in water-acetonitrile mixtures on nanostructured Cu electrode**. *Electrochem Commun* 2015, **61**:74–77, https://doi.org/10.1016/j.elecom.2015.10.003.

78. Gong X, Yu S, Guan M, Zhu X, Xue C: **Pyrene-functionalized polymeric carbon nitride with promoted aqueous–organic biphasic photocatalytic CO_2 reduction**. *J Mater Chem A* 2019, **7**:7373–7379, https://doi.org/10.1039/C8TA09801H.

79. Jutz F, Andanson J-M, Baiker A: **Ionic liquids and dense carbon dioxide: a beneficial biphasic system for catalysis**. *Chem Rev* 2011, **111**:322–353, https://doi.org/10.1021/cr100194q.

80. Mendez MA, Voyame P, Girault HH: **Interfacial photoreduction of supercritical CO_2 by an aqueous catalyst**. *Angew Chem Int Ed* 2011, **50**:7391–7394, https://doi.org/10.1002/anie.201100828.

81. Voyame P, Toghill KE, Mendez MA, Girault HH: **Photoreduction of CO_2 using $[Ru(bpy)_2(CO)L]^{n+}$ catalysts in biphasic solution/supercritical CO_2 systems**. *Inorg Chem* 2013, **52**, 10949, https://doi.org/10.1021/ic401031j. –10957.

82. Shahid UB, Chen Y, Gu S, Li W, Shao M: **Electrochemical nitrogen reduction: an intriguing but challenging quest**. *Trends Chem* 2022, **4**:142–156, https://doi.org/10.1016/j.trechm.2021.11.007.

83. Zhang W, Zhang J, Fan S, Zhang L, Liu C, Liu J: **Oxygen reduction catalyzed by bilirubin oxidase and applications in biosensors and biofuel cells**. *Microchem J* 2022, **183**, 108052, https://doi.org/10.1016/j.microc.2022.108052.

84. Scheiblbrandner S, Csarman F, Ludwig R: **Cellobiose dehydrogenase in biofuel cells**. *Curr Opin Biotechnol* 2022, **73**:205–212, https://doi.org/10.1016/j.copbio.2021.08.013.